NASA Technical Memorandum 104221

ADAPTIVE UNSTRUCTURED MESHING FOR THERMAL STRESS ANALYSIS OF BUILT-UP STRUCTURES

PRAMOTE DECHAUMPHAI

FEBRUARY 1992

National Aeronautics and Space Administration
Langley Research Center
Hampton, Virginia 23665

ERRATA

NASA Technical Memorandum 104221

Adaptive Unstructured Meshing for Thermal Stress Analysis of Built-Up Structures

Pramote Dechaumphai

February 1992

Attached is a new copy of NASA Technical Memorandum 104221. The wrong Report Documentation Page was printed in the report which was previously sent to you. Please destroy all copies of the report that you previously received.

Issued March 1992

ADAPTIVE UNSTRUCTURED MESHING FOR THERMAL STRESS ANALYSIS OF BUILT-UP STRUCTURES

Pramote Dechaumphai*
NASA Langley Research Center
Hampton, Virginia

Abstract

An adaptive unstructured meshing technique for mechanical and thermal stress analysis of built-up structures has been developed. A triangular membrane finite element and a new plate bending element are evaluated on a panel with a circular cutout and a frame stiffened panel. The adaptive unstructured meshing technique, without a priori knowledge of the solution to the problem, generates clustered elements only where needed. An improved solution accuracy is obtained at a reduced problem size and analysis computational time as compared to the results produced by the standard finite element procedure.

Nomenclature

A	finite element area
[B]	strain-displacement matrix
[C]	material stiffness matrix
D	bending rigidity
E	modulus of elasticity
{F}	load vector
h	nodal spacing
[K]	stiffness matrix
M	bending moment
[N]	element interpolation function matrix
p	pressure
$\{S_1\}$, $\{S_2\}$	vector of stress components
T	temperature
T_o	reference temperature for zero stress
t	element thickness
u, v, w	displacement components
x, y, z	local coordinate directions
X, Y, Z	global coordinate directions
α	coefficient of thermal expansion
$\{\alpha\}$	vector of coefficients of thermal expansion
$\{\delta\}$	vector of element nodal unknowns
$\{\varepsilon\}$	vector of strain components
λ	eigenvalue
ν	Poisson's ratio
ϕ	key parameter for remeshing
$\sigma_x, \sigma_y, \tau_{xy}$	stress components
σ_1, σ_2	principal stress components

Subscripts

b	bending
m	membrane
p	pressure
T	thermal

Superscripts

T	transpose

Introduction

Accurate prediction of the structural response induced by both mechanical and thermal loads is an important factor in the design of many structures. Intense pressure and heat transfer rates may produce severe stresses that reduce the structural performance and may cause structural failure. Research is underway to improve the efficiency and accuracy of the structural analysis procedure.

An adaptive unstructured meshing technique[1] has been shown to improve the efficiency and accuracy[2] of the high speed flow analysis, the thermal, and structural analyses of continuum structures in two dimensions by the finite element method. The technique generates a new mesh based on the solution obtained from an earlier mesh. The new mesh consists of small elements in the regions with large changes in solution gradients and large elements in other regions where the gradient changes are small. Because the technique generates proper element sizes automatically, it is especially suitable for complex problems where a priori knowledge of the solutions does not exist.

Herein, the technique has been extended to construct adaptive meshes for structural analysis of "built-up" structures. Such structures are commonly modelled by using two-dimensional membrane and plate bending finite elements. A new triangular plate bending element to be used with the adaptive unstructured meshes for efficient thermal stress solution is introduced in this paper. The paper, however, will concentrate on the evaluation of the adaptive unstructured meshing technique for providing solution accuracy as well as increasing computational efficiency for thermal stress analysis of structures.

The governing differential equations for predicting the structural response due to both thermal and mechanical loads will be presented first. The triangular membrane element with temperature distribution over the element and a new triangular plate bending element with temperature gradient through the element thickness will be described. The corresponding finite element equations and the associated element matrices will be derived and presented. The basic concepts of the adaptive unstructured meshing technique and the selection of the meshing parameters used for

*Aerospace Technologist, Aerothermal Loads Branch, Structural Mechanics Division

construction of new meshes will be explained. Before applying the adaptive unstructured meshing technique to complex problems, the technique will be evaluated for the stress analysis of a panel with a circular cutout where the exact solution is available. The performance of the new triangular plate bending element under the thermal load will then be evaluated using an example of a plate with temperature gradient through its thickness for which the exact solution is also available. Finally the adaptive unstructured meshing technique for built-up structures will be evaluated by the thermal stress analysis of convectively-cooled intersecting frame stiffened panels in which the adaptive mesh solution will be compared with a fine mesh solution.

Thermal Stress Analysis Procedure

Governing Equations

The equations for the in-plane deformation and the transverse deflection of a plate that lies in a local x-y coordinate system are briefly described herein.

In-Plane Deformation. The equations for the in-plane deformation are given by the two-dimensional equilibrium equations in the form,

$$\frac{\partial}{\partial x}\{S_1\} + \frac{\partial}{\partial y}\{S_2\} = 0 \qquad (1)$$

where the vectors $\{S_1\}$ and $\{S_2\}$ consist of the stress components given by,

$$\begin{aligned} \{S_1\} &= [\,\sigma_x \quad \tau_{xy}\,]^T \\ \{S_2\} &= [\,\tau_{xy} \quad \sigma_y\,]^T \end{aligned} \qquad (2)$$

The stress components are related to the strain components and the temperature by the generalized Hooke's law,

$$\{\sigma\} = [C_m]\{\varepsilon\} - [C_m]\{\alpha\}(T(x,y) - T_o) \qquad (3)$$

where $\{\sigma\}$ contains the stress components σ_x, σ_y, and τ_{xy}, $[C_m]$ is the material stiffness matrix, and $\{\alpha\}$ is the vector of the coefficients of thermal expansion. For the plane stress case, these material matrices are given in Ref. 3. The vector of the strain components is related to the displacement gradients given by,

$$\{\varepsilon\} = [\frac{\partial u}{\partial x} \quad \frac{\partial v}{\partial y} \quad \frac{\partial u}{\partial y} + \frac{\partial v}{\partial x}]^T \qquad (4)$$

Transverse Deflection. The equation for the transverse deflection in the z-direction normal to the x-y plane of the plate is given by the equilibrium equation[4] in the form,

$$D(\frac{\partial^4 w}{\partial x^4} + 2\frac{\partial^4 w}{\partial x^2 \partial y^2} + \frac{\partial^4 w}{\partial y^4}) = -\frac{1}{1-\nu}(\frac{\partial^2 M_T}{\partial x^2} + \frac{\partial^2 M_T}{\partial y^2}) + p(x,y) \qquad (5)$$

where $D = Et^3/12(1-\nu^2)$ is the bending rigidity, $p(x,y)$ is the transverse pressure, and M_T is the thermal moment defined by,

$$M_T = E\alpha\int_{-t/2}^{t/2}(T(z) - T_o)\,z\,dz \qquad (6)$$

Derivation of Finite Element Equations

The Constant Strain Triangle (CST) and the Discrete Kirchoff Triangle (DKT) finite elements are used for the in-plane deformation and the transverse deflection, respectively.

Constant Strain Triangle (CST). The three-node CST element assumes a linear displacement distribution[3] over the element. The element equations can be derived by applying the method of weighted residuals to the governing differential equation, Eq. (1), which leads to the element equations in the form,

$$[K_m]\{\delta_m\} = \{F\} + \{F_m\} \qquad (7)$$

where the vector $\{\delta_m\}$ contains the element nodal unknowns of the in-plane displacements in the element local x-y coordinate directions. There are two in-plane displacements per node or six in-plane displacements per element. The element stiffness matrix, $[K_m]$, that appears in Eq. (7) is defined by,

$$[K_m] = [B_m]^T[C_m][B_m]\,t\,A \qquad (8)$$

where the strain-displacement interpolation matrix, $[B_m]$, is given in Ref. 3. The first vector, $\{F\}$, on the right-hand-side of Eq. (7) contains the applied mechanical forces at element nodes. The second vector, $\{F_m\}$, consists of the equivalent nodal forces due to the thermal load. This second vector is defined by,

$$\{F_m\} = [B_m]^T[C_m]\{\alpha\}(T_{avg} - T_o)\,t\,A \qquad (9)$$

where $T_{avg} = \int_A T(x,y)\,dA / A$.

Discrete Kirchoff Triangle (DKT). The three-node DKT element assumes a cubic distribution of the transverse deflection[5] over the element. The element equations can be derived by applying the method of weighted residuals to the plate bending equations, Eq. (5), which leads to the element equations in the form,

$$[K_b]\{\delta_b\} = \{F_p\} + \{F_b\} \qquad (10)$$

where the vector $\{\delta_b\}$ contains the element nodal unknowns of the transverse deflections and the rotations (slopes). Each node has a transverse deflection in the element local z-coordinate direction and two rotations about the element local x-y coordinate directions. Thus there are nine degrees of freedom per element. The performance of the element has been evaluated thoroughly in Ref. 6 using several benchmark problems for bending of plates under mechanical loading. However, the performance of the element under thermal

loading has not been evaluated. Without thermal loading, only the element stiffness matrix, $[K_b]$, and the nodal force vector due to the applied pressure, $\{F_p\}$, that appear in the element equations, Eq. (10), are needed. These matrices are defined by,

$$[K_b] = \int_A [B_b]^T [C_b] [B_b] \, dA \qquad (11)$$

$$\{F_p\} = \int_A [N_b]^T p \, dA \qquad (12)$$

where the strain-displacement interpolation matrix, $[B_b]$, the plate material stiffness matrix, $[C_b]$, and the plate element interpolation function matrix, $[N_b]$, are given in Refs. 5-6. The above two element matrices, $[K_b]$ and $\{F_p\}$, can be evaluated in closed form (i.e. numerical integration is not required) and the details of the derivation are given in Refs. 6-7.

With the presence of thermal loading, the vector of the equivalent nodal forces, $\{F_b\}$, due to the thermal moment is included in the element equations, Eq. (10). This additional vector is defined by,

$$\{F_b\} = \int_A [B_b]^T \{M\} \, dA \qquad (13)$$

where

$$\{M\} = [M_T \quad M_T \quad 0]^T \qquad (14)$$

The thermal moment M_T is defined in Eq. (6). The vector of the equivalent nodal forces due to thermal loading, $\{F_b\}$, above can also be derived in closed form. For an element with arbitrary temperature distribution through the plate thickness, $T = T(z)$, this vector, $\{F_b\}$, is

$$\{F_b\} = M_T [G]^T \begin{Bmatrix} 1 \\ 1 \\ 0 \end{Bmatrix} \qquad (15)$$

where the matrix [G] has been derived and given in the Appendix.

Note that, for general built-up structures, elements can be arbitrarily oriented in three dimensions. Transformation of these element matrices from a local x-y-z coordinate system to a global X-Y-Z coordinate system is required before assembling them to obtain a set of simultaneous equations. In such a global X-Y-Z coordinate system, each node has six degrees of freedom which are the three translations and the three rotations. The matrix transformation procedure, however, can be easily worked out and is not presented herein for brevity.

Adaptive Unstructured Remeshing Procedure

Remeshing Strategy

The basic idea of adaptive unstructured remeshing[1] is to construct a completely new mesh based on key parameters from the solution obtained on a previous mesh. The new mesh will have small elements (short nodal spacings) in regions of large changes in solution gradients and large elements (large nodal spacings) in regions where the gradient changes are small. Proper nodal spacings used for constructing a new mesh are determined by following a procedure analogous to the solid mechanics concept of finding the principal stresses, σ_1 and σ_2, from a given state of stresses, σ_x, σ_y, and τ_{xy}, i.e.,

$$\begin{bmatrix} \sigma_x & \tau_{xy} \\ \tau_{xy} & \sigma_y \end{bmatrix} \Rightarrow \begin{bmatrix} \sigma_1 & 0 \\ 0 & \sigma_2 \end{bmatrix} \qquad (16)$$

At a typical node in the previous mesh, the second derivatives of the key parameter for remeshing, ϕ, (analogous to the stress components in Eq. (16)) are computed and the two eigenvalues (analogous to the principal stresses) are then determined,

$$\begin{bmatrix} \frac{\partial^2 \phi}{\partial x^2} & \frac{\partial^2 \phi}{\partial x \, \partial y} \\ \frac{\partial^2 \phi}{\partial x \, \partial y} & \frac{\partial^2 \phi}{\partial y^2} \end{bmatrix} \Rightarrow \begin{bmatrix} \lambda_1 & 0 \\ 0 & \lambda_2 \end{bmatrix} \qquad (17)$$

The larger eigenvalue, $\lambda = \max(\lambda_1, \lambda_2)$, is then selected for that node and the same process is repeated for all the other nodes in the previous mesh. Proper nodal spacings, denoted by h, used for constructing a new mesh are then determined from an equidistribution condition[1],

$$\lambda h^2 = \text{constant} = \lambda_{max} h_{min}^2 \qquad (18)$$

where λ_{max} is the largest eigenvalue of all the nodes in the previous mesh and h_{min} is the specified minimum nodal spacing for the new mesh.

The second derivatives of the key parameter, ϕ, are determined using the following procedure. The first derivative (e.g. with respect to x) is assumed to vary over an element in the form,

$$\frac{\partial \phi(x,y)}{\partial x} = [N] \left\{ \frac{\partial \phi}{\partial x} \right\} \qquad (19)$$

where the vector on the right-hand-side contains the unknown nodal values of the first derivatives. These unknowns are obtained by solving,

$$\int_A \{N\} [N] \, dA \left\{ \frac{\partial \phi}{\partial x} \right\} = \int_A \{N\} \, dA \, \frac{\widehat{\partial \phi}}{\partial x} \qquad (20)$$

where $\widehat{\partial \phi / \partial x}$ is the computed uniform element gradient. The process is repeated to determine the second derivative $\partial^2 \phi / \partial x^2$. Determination of the other second derivatives which appear in Eq. (17) is performed in the same fashion.

Remeshing Parameters

The adaptive remeshing technique requires a selection of proper key parameters (ϕ in Eq. (17)). For structural problems under mechanical load alone, stress is an appropriate choice. However, the key parameter representing the stress should be a scalar quantity which takes into account all the stress components, such as the Von Mises stress defined in two dimensions by,

$$\sigma_{\text{Von Mises}} = \frac{1}{\sqrt{2}}\sqrt{(\sigma_x - \sigma_y)^2 + \sigma_x^2 + \sigma_y^2 + 6\tau_{xy}^2} \qquad (21)$$

For structural problems under both mechanical and thermal loads, the structural temperature and the Von Mises stress should be used as the key parameters for remeshing simultaneously so that the mesh generated can accurately represent the prescribed temperature distribution and can capture the high thermal stress as well as the mechanical stress concentration.

Applications

Three example problems are presented. The first example demonstrates the effectiveness of the adaptive unstructured remeshing technique on a plane stress problem using CST elements. The second example is used to evaluate the performance of the triangular DKT plate bending element under thermal loading. The third example combines both the CST and DKT elements and demonstrates the capability of the adaptive unstructured remeshing technique for a built-up structure.

Panel With Circular Cutout

A panel with a circular cutout, shown in Fig. 1, is an ideal structure to demonstrate the capability of the adaptive unstructured meshing technique because closed-form solutions[8] are available. The panel is subjected to an applied uniform stress (σ_o) of 10 ksi in the longitudinal y-direction (see figure). The exact normal stress (σ_y) distribution along the x-direction at y=0 is given by,

$$\sigma_y = \frac{\sigma_o}{2}\left(2 + \frac{a^2}{x^2} + 3\frac{a^4}{x^4}\right) \qquad (22)$$

where a is the radius of the circular cutout. The peak stress ($3\sigma_o$) of 30 ksi occurs at the boundary of the cutout (point A in the figure).

Due to symmetry, a quarter of the panel is analyzed. The initial unstructured mesh consisted of 184 nodes and 306 triangles as shown in Fig. 2(a). Details of the mesh near the cutout are shown in Fig. 2(b). With this mesh, a plane stress analysis with CST elements was performed to predict the panel deformation and the stress distributions. The contours of the normal stress (σ_y) distribution in the longitudinal y-direction near the cutout are shown in Fig. 2(c). The peak predicted stress (σ_y) at the cutout is 19.5 ksi compared to the exact peak stress of 30 ksi. The 35% error in the peak stress is due to the large elements used near the cutout region.

The Von Mises stresses obtained from this initial mesh solution are used as the key parameter for the adaptive remeshing. The new adaptive mesh, shown in Fig. 3(a), has approximately 20% fewer nodes and elements (149 nodes and 250 triangles) than the initial mesh. However, small elements are concentrated in the region of high stress gradients near the cutout (shown in Fig. 3(b)) to provide a more accurate stress solution. The normal stress (σ_y) contours obtained with this mesh are shown in Fig. 3(c). The peak predicted stress (σ_y) at the cutout is now 28.5 ksi which is only 5% lower than the exact level of 30 ksi.

The normal stress (σ_y) distributions along the x-direction at y=0 obtained from the initial and the adaptive meshes are compared with the exact stress distribution in Fig. 4. By defining a percentage error based on the L_2 norm of the form,

$$\%\ \text{error} = \frac{\left(\int_a^b [(\sigma_y)_{\text{Exact}} - (\sigma_y)_{\text{F.E.}}]^2\, dx\right)^{1/2}}{\left(\int_a^b [(\sigma_y)_{\text{Exact}}]^2\, dx\right)^{1/2}} \times 100 \qquad (23)$$

the figure shows that the solution error was reduced from 17% to 2% with one adaptive remesh. In addition, increased solution accuracy was obtained with fewer unknowns because small elements are concentrated in the region of high stress gradients near the cutout and large elements are generated in other regions.

It is important to note that the adaptive meshing technique automatically generates refined elements in the regions of high stresses. A priori knowledge of the solution to the problem (e.g. high stress regions that require refined elements) is not needed before performing the analysis. The technique thus provides an advantage over the standard finite element procedure especially for more complex problems or larger structures (such as the structure which will be presented in the last example) where a priori knowledge of the solution does not exist.

Plate Bending Due To Thermal Load

The unconstrained aluminum plate with a temperature gradient through its thickness, shown in Fig. 5, is a simple example for evaluating the performance of the DKT plate bending element. The exact solution[4] for the transverse deflection is given by,

$$w(x,y) = -\frac{3 M_T}{4 E t^3}(x^2 + y^2) \qquad (24)$$

where M_T is the thermal moment defined in Eq. (6). For a linear temperature distribution through the plate thickness with a temperature T_{Top} on the top surface and T_{Bottom} on the bottom surface, the thermal moment is given by,

$$M_T = \frac{E \alpha t^2}{12 (1 - \nu)}(T_{Top} - T_{Bottom}) \qquad (25)$$

Due to symmetry, a quarter of the plate is analyzed. The finite element model consists of 32 DKT plate bending elements and 25 nodes with 5 nodes equally spaced in the x and y directions (See Fig. 5.). The top and bottom surface temperatures are 630°R and 530°R, respectively. A comparison of the finite element and the exact transverse deflection solutions along the x-direction at y=0 is shown in Fig. 6. The figure shows that the DKT plate bending elements essentially provide an exact transverse deflection solution.

As described earlier, all the DKT plate bending element matrices are evaluated in closed form. This simplifies the programming task, reduces the computational effort and eliminates numerical error that may occur in generating such element matrices. In addition, reference 6 has demonstrated the effectiveness of this element for providing solution accuracy for plate bending problems under different types of the mechanical load. The example presented herein demonstrates the performance and the capability of the DKT element for providing accurate structural response due to the thermal load. The next example will combine the CST elements (used in the first example) and the DKT elements (used in this example) with the adaptive unstructured meshing technique for thermal stress analysis of a more complex built-up structure.

Thermal Stress in Intersecting Panels

To demonstrate the capability of the adaptive unstructured meshing technique for thermal stress analysis of more complex structures, a three-dimensional structure which represents a scramjet engine inlet is considered. The structure experiences high heat transfer rates from the impingement of an oblique shock from the vehicle forebody as illustrated in Fig. 7. The localized heat transfer rates result in high temperature gradients and their attendant thermal stresses in the engine panel. A typical "built-up" engine inlet structure, shown in the lower right corner of the figure, may consist of panels and stiffeners and may be actively cooled. To perform the thermal stress analysis of such a structure, a finite element model consisting of two-dimensional plate bending and membrane elements for the panels and the stiffeners is required. Note that, in constructing such a finite element model, the same nodal discretization is generally required along the interface between the stiffeners and the panels. Such a discretization constraint, combined with the requirement of placing fine elements at the high thermal stress regions for an accurate thermal stress solution, is tedious if done nonadaptively. Furthermore, several modelling iterations may be needed before achieving the desired solution accuracy.

For the purpose of demonstrating that the thermal stress solution accuracy can be improved by using the adaptive unstructured meshing technique, both the structural temperature distribution and the structural boundary conditions are prescribed as shown in Fig. 8. The structural boundary conditions are applied such that the intersecting panels can move freely in the global X, Y, and Z directions as illustrated in the figure. The prescribed temperature distribution simulates the structural temperature response from the shock impingement illustrated in Fig. 7. The distribution is assumed to decay radially as a quadratic function from a peak of 700°R (at the centers of the two "hot spots") to 50°R (in the regions away from the two hot spots) as illustrated in Fig. 8. The temperature of 50°R is representative of the coolant temperature.

For most thermal stress problems, high compressive stresses normally occur at the high temperature and temperature gradient regions. Refined finite elements are thus needed in these regions. For more complex structures, high thermal stresses may also occur in other regions that have lower temperature or temperature gradients depending on the complexity of the structures and how they are constrained. Thus, in the standard finite element analysis procedure, a relatively fine finite element model is normally employed first to identify such high thermal stress regions. An example of a fine finite element model is shown in Fig. 9(a) which consists of 3,168 nodes (19,008 degrees of freedom) and 6,114 triangular elements.

The predicted thermal stress distribution in the Y-direction superimposed on the deformed geometry (greatly exaggerated), obtained from this fine finite element model, is shown in Fig. 9(b). As expected, high compressive stresses with a magnitude of 25 ksi occur at the two hot spots. However, a tensile stress of 54 ksi occurs between these two regions. Such phenomenon may not be anticipated before analyzing the problem or before constructing the finite element model. This example demonstrates a need for an automated analysis procedure that can provide an accurate solution without a priori knowledge of the solution.

The solution for this fine finite element model requires a computational time of approximately 13 CPU hours on a VAX-8550 computer. This computational time can be reduced significantly by placing larger elements in the regions away from the hot spot regions. As mentioned earlier, construction of a finite element model with different element sizes while maintaining the same nodal discretization along the interface between various structural components is difficult. Furthermore, it is also difficult to construct a finite element model using all the four-node quadrilateral elements to satisfy such requirements and to achieve smooth transition of element sizes from the fine to the coarse mesh regions. These difficulties can be alleviated and the analysis computational time can be reduced by the adaptive unstructured meshing technique described next.

Application of the adaptive unstructured meshing technique starts by constructing a fairly uniform but coarse initial mesh as shown in Fig. 10. This initial mesh consists of 547 nodes (3,282 degrees of freedom) and 994 triangular elements, which is approximately 1/6th the size of the previous mesh. The predicted thermal stress distribution in the Y-direction superimposed on the deformed geometry is shown in Fig. 11. The peak compressive stress at the two hot spots is 20 ksi while the peak predicted tensile stress between the two hot spots is 33 ksi (approximately 40% lower than the fine mesh solution shown in Fig. 9). The computational time required by this initial mesh is about 15 minutes on the same VAX-8550 computer.

The temperature and the stress distribution (in form of the Von Mises stress given by Eq. (21)) obtained from the initial mesh are used as the meshing parameters to automatically construct a new adaptive mesh. The new adaptive mesh, shown in Fig. 12, has slightly fewer nodes and elements (528 nodes and 989 elements) than the initial mesh. However, smaller

elements are concentrated in the high stress regions on both the panels and the stiffeners. Larger elements are generated in other regions to reduce the problem size and thus the computational time. The predicted thermal stress distribution in the Y-direction superimposed on the deformed geometry is shown in Fig. 13. The figure shows that the adaptive mesh model provides the same stress solution level as obtained from the fine mesh model shown in Fig. 9 (i.e. the peak predicted tensile stress of 54 ksi is between the two hot spots that have compressive stresses of 25 ksi). The total CPU time used for the entire adaptive analysis procedure is approximately 30 minutes, i.e. 15 minutes each for the solutions on the initial and the adaptive mesh and approximately a minute for constructing the two meshes. This total CPU time therefore is 1/25th the CPU time required by the fine mesh model.

The adaptive mesh model shown in Fig. 12 also highlights the ease of constructing a finite element model by using triangles. These triangles provide smooth transition of the element sizes from refined to coarse mesh regions, i.e. in the neighborhood of the hot spots as shown in the figure. The smooth element transition provides a comparable stress distribution to the fine mesh solution as indicated by comparing the stress contours obtained from the adaptive mesh model (Fig. 13) and the fine mesh model (Fig. 9). This last application demonstrates that, without a priori knowledge of the solution, the adaptive unstructured remeshing technique provides the same thermal stress solution accuracy as the fine mesh solution but at a reduced analysis computational cost.

Concluding Remarks

An adaptive unstructured remeshing technique for thermal stress analysis of built-up structures has been developed. The technique generates a new mesh based on the solution obtained from a previous mesh. The new mesh consists of small elements in regions of large change in the stress gradients and large elements in other regions where the gradient changes are small. The finite element thermal stress formulation for the triangular membrane (CST) and plate bending (DKT) elements under both mechanical and thermal loads is presented. All the element matrices were derived in closed form to simplify the programming task, reduce the computational time and eliminate error associated with the numerical integration. To construct a new adaptive mesh, proper nodal spacings are determined from the meshing indicators that are represented by the second derivatives of the selected meshing parameters. The higher the second derivatives computed, the smaller the element sizes generated. The meshing parameters are selected according to the type of the problems. For example, both the temperature and Von Mises stress are used together as the meshing parameters for thermal stress problems so that refined elements are generated in the regions of high thermal stress and mechanical stress concentration.

The two applications presented in this paper demonstrate that the adaptive unstructured meshing technique: (1) reduces modelling effort because a priori knowledge of the solution is not required; (2) provides improved solution accuracy by adapting the mesh to the physics of the solutions; (3) reduces the problem size by automatically generating small elements in the regions with high solution gradients and large elements in the other regions; and (4) provides smooth solution transition from fine to coarse mesh regions with the use of triangular elements.

Appendix

The vector of the equivalent nodal forces due to the thermal load, $\{F_b\}$, for the DKT plate bending element given in Eq. (15) can be evaluated in closed form. This vector includes the matrix [G] given by,

$$[G] = \frac{1}{6}\begin{bmatrix} y_{31}[G_{11}] + y_{12}[G_{12}] \\ -x_{31}[G_{21}] - x_{12}[G_{22}] \\ -x_{31}[G_{11}] - x_{12}[G_{12}] + y_{31}[G_{21}] + y_{12}[G_{22}] \end{bmatrix}$$

The coefficients x_{ij} and y_{ij}, i, j=1, 2, 3, are defined in terms of the element nodal coordinates by,

$$x_{ij} = x_i - x_j ; \qquad y_{ij} = y_i - y_j$$

The row matrices, $[G_{ij}]$, i,j=1,2, that appear in the matrix [G] above are given by,

$$[G_{11}] = \begin{bmatrix} p_5 & -q_5 & -r_5 \\ p_4 & q_4 & r_4 \\ -p_4-p_5 & q_4-q_5 & r_4-r_5 \end{bmatrix}$$

$$[G_{12}] = \begin{bmatrix} -p_6 & -q_6 & -r_6 \\ p_4+p_6 & q_4-q_6 & r_4-r_6 \\ -p_4 & q_4 & r_4 \end{bmatrix}$$

$$[G_{21}] = \begin{bmatrix} t_5 & 3-r_5 & q_5 \\ t_4 & -3+r_4 & -q_4 \\ -t_4-t_5 & r_4-r_5 & -q_4+q_5 \end{bmatrix}$$

$$[G_{22}] = \begin{bmatrix} -t_6 & 3-r_6 & q_6 \\ t_4+t_6 & r_4-r_6 & -q_4+q_6 \\ -t_4 & -3+r_4 & -q_4 \end{bmatrix}$$

The coefficients p_k, q_k, r_k and t_k, k = 4, 5, 6 in the row matrices, $[G_{ij}]$, above are defined by,

$$p_k = -6\, x_{ij} / l_{ij}^2 ; \qquad q_k = 3\, x_{ij}\, y_{ij} / l_{ij}^2$$
$$r_k = 3\, y_{ij}^2 / l_{ij}^2 ; \qquad t_k = -6\, y_{ij} / l_{ij}^2$$

where $l_{ij}^2 = x_{ij}^2 + y_{ij}^2$ and k = 4, 5, 6 for ij = 23, 31, 12, respectively.

Intersecting Panels Dimensions

The size of the copper intersecting panels used in the thermal stress analysis in the last example is assumed to be 6 x 10 x 4 inches in the X, Y, and Z directions (see Fig. 8), respectively.

References

1. Peraire, J., Vahdati, M., Morgan, K. and Zienkiewicz, O. C., "Adaptive Remeshing for Compressible Flow Computations," Journal of Computational Physics, Vol. 72, 1987, pp. 449-466.

2. Dechaumphai, P., "Evaluation of an Adaptive Unstructured Remeshing Technique for Integrated Fluid-Thermal-Structural Analysis," Journal of Thermophysics and Heat Transfer, Vol. 5, No. 4, 1991, pp. 599-606.

3. Huebner, K. H. and Thornton, E. A., The Finite Element Method for Engineers, John Wiley & Sons, Inc. New York, 1982.

4. Boley, B. A. and Weiner, J. H., Theory of Thermal Stresses, John Wiley & Sons, Inc. New York, 1960.

5. Stricklin, J. A., Haisler, W. E., Tisdale, P. R. and Gunderson, R., "A Rapidly Converging Triangular Plate Element," AIAA Journal, Vol. 7, No. 1, 1969, pp. 180-181.

6. Batoz, J. L., Bathe, K. J. and Ho, L. W., "A Study of Three-Node Triangular Plate Bending Elements," International Journal for Numerical Methods in Engineering, Vol. 15, 1980, pp. 1771-1812.

7. Jeyachandrabose, C. and Kirkhope, J., "An Alternative Explicit Formulation for the DKT Plate-Bending Element," International Journal for Numerical Methods in Engineering, Vol. 21, 1985, pp. 1289-1293.

8. Timoshenko, S. P. and Goodier, J. N., Theory of Elasticity, Third Edition, McGraw-Hill Book Co., New York, 1934, pp. 90-97.

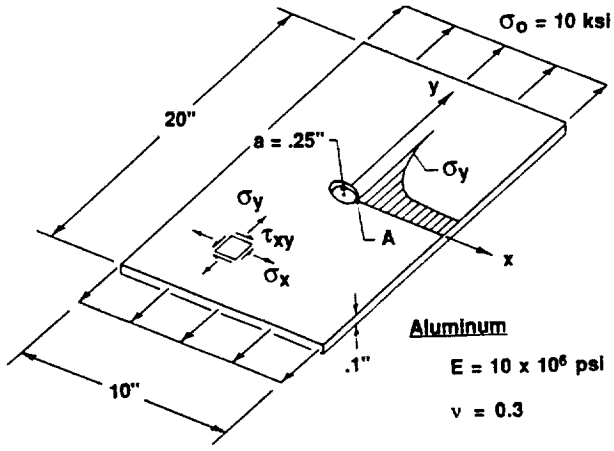

Fig. 1 Schematic of a panel with a circular cutout subjected to an applied in-plane stress.

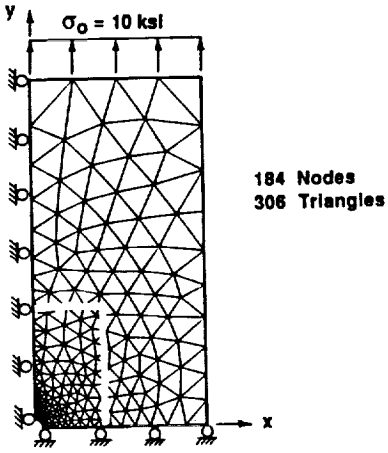

(a) Initial mesh

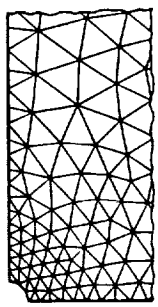

(b) Detailed mesh near the cutout

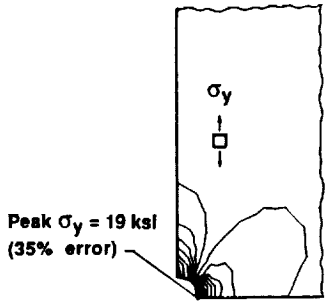

(c) Predicted stress contours

Fig. 2 Initial finite element mesh for the panel with a circular cutout and the predicted stress contours.

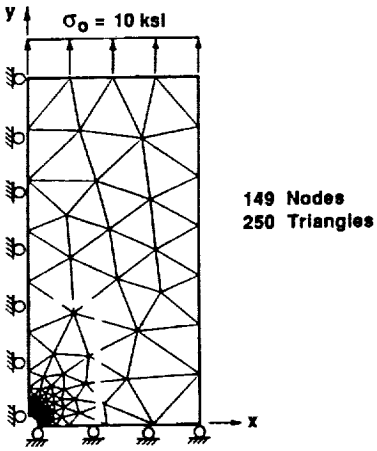

(a) Adaptive mesh

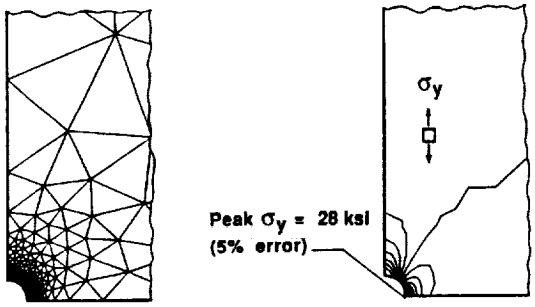

(b) Detailed mesh near the cutout

(c) Predicted stress contours

Fig. 3 Adaptive finite element mesh for the panel with a circular cutout and the predicted stress contours.

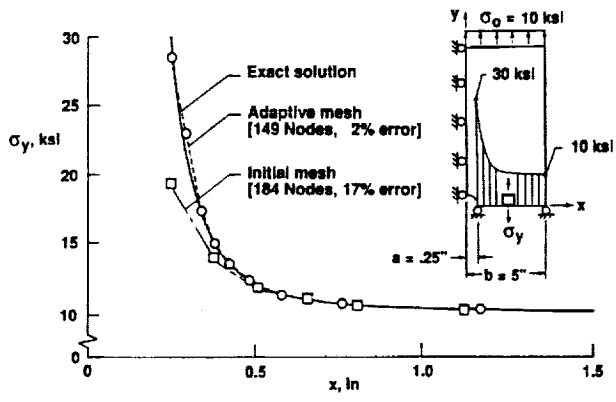

Fig. 4 Comparison of the predicted finite element and the exact stress distributions along the x-direction at y=0 for the panel with a circular cutout.

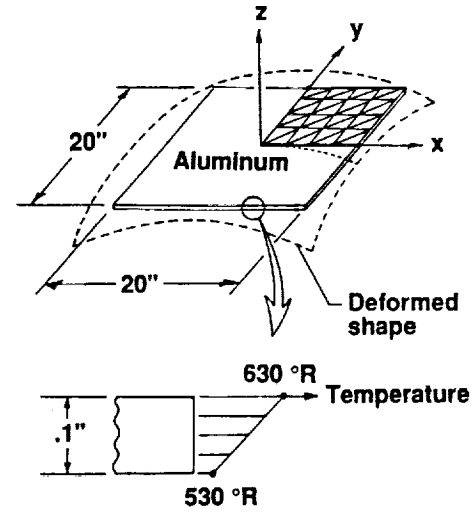

Fig. 5 Schematic of an unconstrained plate subjected to linear temperature distribution through its thickness.

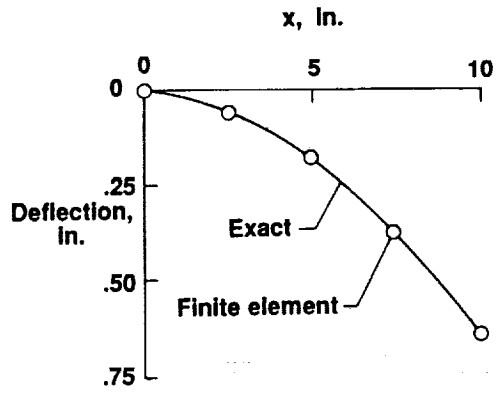

Fig. 6 Comparison of the predicted finite element and the exact transverse deflections along the x-direction at y=0 for the plate with linear temperature distribution through its thickness.

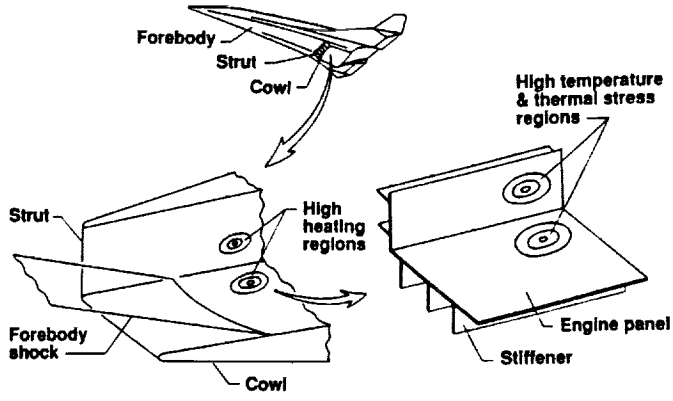

Fig. 7 Schematic of high heating and thermal stress regions on a scramjet engine inlet represented by a structure with intersecting panels.

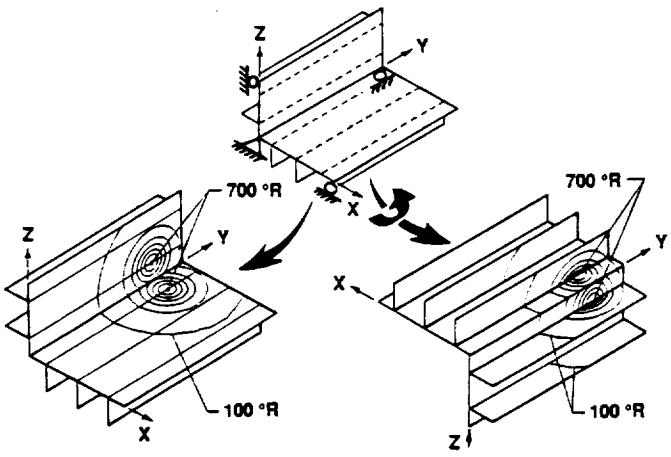

Fig. 8 Structural boundary conditions and the prescribed temperature distributions for the intersecting panels.

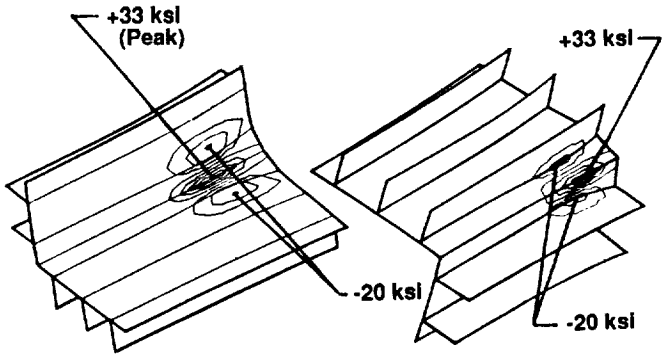

Fig. 11 Predicted axial stress contours from the initial finite element mesh on deformed intersecting panel configuration.

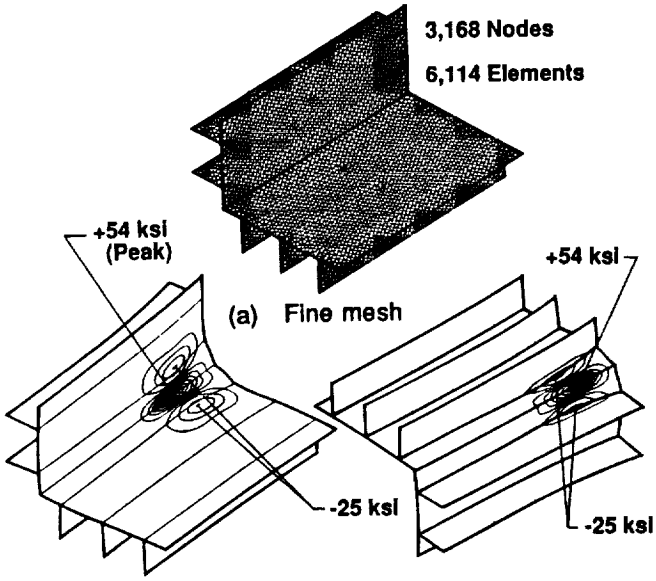

(b) Predicted axial stress contours

Fig. 9 Standard fine finite element mesh and the predicted axial stress contours on deformed configuration.

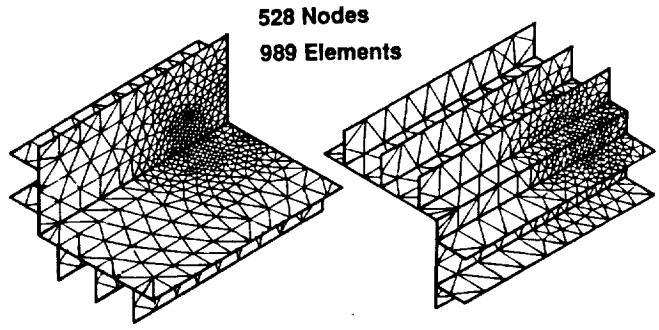

Fig. 12 Adaptive unstructured finite element mesh for the intersecting panels.

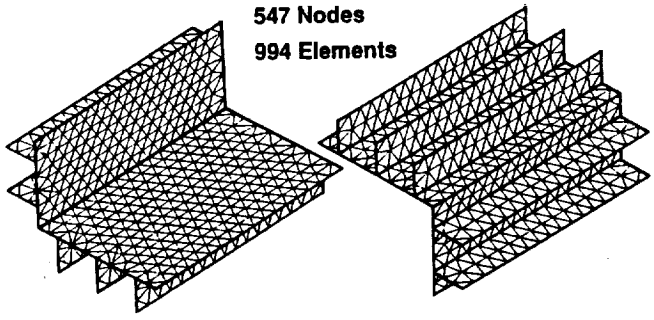

Fig. 10 Initial finite element mesh for the intersecting panels.

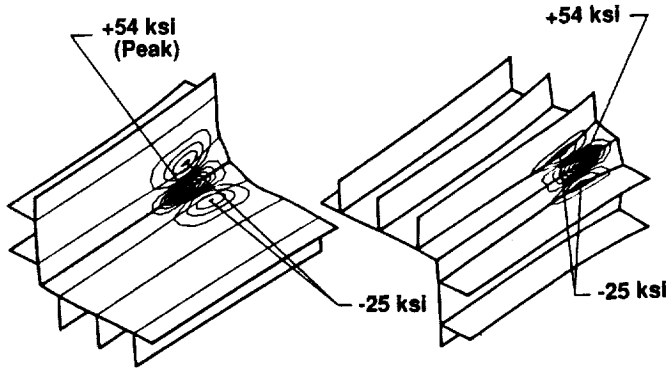

Fig. 13 Predicted axial stress contours from the adaptive finite element mesh on deformed intersecting panel configuration.

REPORT DOCUMENTATION PAGE

Form Approved
OMB No. 0704-0188

1. AGENCY USE ONLY *(Leave blank)*	2. REPORT DATE	3. REPORT TYPE AND DATES COVERED
	February 1992	Technical Memorandum

4. TITLE AND SUBTITLE

Adaptive Unstructured Meshing for Thermal Stress Analysis of Built-Up Structures

5. FUNDING NUMBERS

506-43-31-03

6. AUTHOR(S)

Pramote Dechaumphai

7. PERFORMING ORGANIZATION NAME(S) AND ADDRESS(ES)

NASA Langley Research Center
Hampton, VA 23665-5225

8. PERFORMING ORGANIZATION REPORT NUMBER

9. SPONSORING/MONITORING AGENCY NAME(S) AND ADDRESS(ES)

National Aeronautics and Space Administration
Washington, DC 20546-0001

10. SPONSORING/MONITORING AGENCY REPORT NUMBER

NASA TM-104221

11. SUPPLEMENTARY NOTES

Presented at AIAA 33rd Structures, Structural Dynamics and Materials Conference, Dallas, Texas, April 13-15, 1992.

12a. DISTRIBUTION/AVAILABILITY STATEMENT

Unclassified - Unlimited

Subject Category 39

12b. DISTRIBUTION CODE

13. ABSTRACT *(Maximum 200 words)*

An adaptive unstructured meshing technique for mechanical and thermal stress analysis of built-up structures has been developed. A triangular membrane finite element and a new plate bending element are evaluated on a panel with a circular cutout and a frame stiffened panel. The adaptive unstructured meshing technique, without a priori knowledge of the solution to the problem, generates clustered elements only where needed. An improved solution accuracy is obtained at a reduced problem size and analysis computational time as compared to the results produced by the standard finite element procedure.

14. SUBJECT TERMS

Adaptive Unstructured Grids
Thermal Stress
Finite Element

15. NUMBER OF PAGES

10

16. PRICE CODE

A02

17. SECURITY CLASSIFICATION OF REPORT	18. SECURITY CLASSIFICATION OF THIS PAGE	19. SECURITY CLASSIFICATION OF ABSTRACT	20. LIMITATION OF ABSTRACT
Unclassified	Unclassified	Unclassified	Unlimited